JACS
JOURNAL OF THE AMERICAN CHEMICAL SOCIETY
pubs.acs.org/JACS
Article

Multistate Structure Determination and Dynamics Analysis Reveals a Unique Ubiquitin-Recognition Mechanism in Ubiquitin C-terminal Hydrolase

Mayu Okada,[‡] Yutaka Tateishi,[‡] Eri Nojiri, Tsutomu Mikawa, Sundaresan Rajesh, Hiroki Ogasa, Takumi Ueda, Hiromasa Yagi, Toshiyuki Kohno, Takanori Kigawa, Ichio Shimada, Peter Güntert, Yutaka Ito,* and Teppei Ikeya*

Cite This: J. Am. Chem. Soc. 2025, 147, 29884−29894

Read Online

ACCESS | Metrics & More | Article Recommendations | Supporting Information

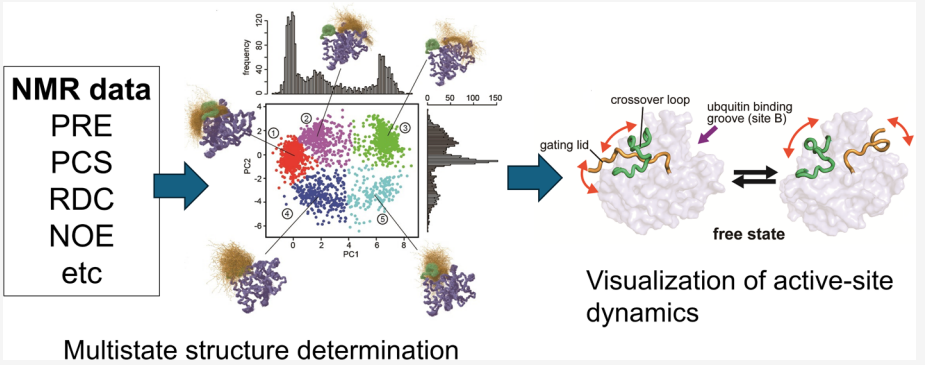

ABSTRACT: Despite accumulating evidence that protein dynamics is indispensable for understanding the structural basis of biological activities, it remains challenging to visualize the spatial description of the dynamics and to associate transient conformations with their molecular functions. We have developed a new NMR protein structure determination method for the inference of multistate conformations using multiple types of NMR data, including paramagnetic NMR and residual dipolar couplings, as well as conventional NOEs. Integration of these data in the structure calculation permits delineating accurate ensemble structures of biomacromolecules. Applying the method to yeast ubiquitin hydrolase 1, we find large dynamics of its N-terminus (gating lid) and crossover loop surrounding the active site for ubiquitin-recognition and proteolysis. The N-terminus (gating lid) moves into and out of the crossover loop, suggesting their underlying functional significance. Our results, including those from biochemical analysis, show that large motion surrounding the active site contributes strongly to the efficiency of the enzymatic activity.

INTRODUCTION

It is well-known that the dynamics of three-dimensional (3D) protein structures enables multiplicity and flexibility of molecular functions. Numerous experimental reports have demonstrated that the functional or binding sites of proteins are often not rigid but rather flexible, allowing multiple roles or adaptive interactions with several other molecules.[1] Intrinsically disordered proteins (IDPs), for example, possess extraordinarily large structural flexibility that confers them unique properties to interact with several other counterparts.[2] Considering that flexible protein structures are susceptible to their surrounding environment, it is crucial to study the molecular motions and 3D structures of proteins at atomic resolution under near-physiological conditions. Nuclear Magnetic Resonance (NMR) spectroscopy is currently the only technique to investigate the dynamics and 3D conformations of proteins at atomic resolution in solution or even in living systems.[3,4] Data from solution NMR includes information on the protein behavior and dynamics as a structural ensemble, and hence various NMR methodologies have been proposed for the extraction of their physical properties from the spectra. For instance, NMR experiments for the quantification of protein dynamics, such as CPMG relaxation dispersion,[5] DEST,[6] and CEST,[7] provide particularly useful information on molecular motion at multiple time scales and lowly populated "excited-state" conformations.

Received: April 16, 2025
Revised: July 17, 2025
Accepted: July 18, 2025
Published: August 6, 2025

However, it remains a challenge to visualize dynamic protein structural ensembles and to elucidate their correlations with molecular functions. To date, several studies have addressed the reconstruction of structural ensembles by extracting dynamical 3D structural information from residual dipolar couplings (RDCs),[8] paramagnetic relaxation enhancements (PREs),[9,10] solvent PREs,[11] and exact nuclear Overhauser effects (eNOEs).[12] However, many of these studies investigated disordered proteins, and did not perform *de novo* protein structure determination exclusively from experimental data, or were applied to small proteins using only one or two types of NMR data. The NOE-type experiments provide distance information from a large number of hydrogen pairs in a molecule, which is necessary to obtain the complete structure of a protein containing detailed side-chain coordinates, but cover only short distances up to 5−6 Å. On the other hand, monitoring large dynamic conformations with high reliability also requires structural information for longer distances.[13] Paramagnetic effects, PREs and pseudcontact shifts (PCSs), provide long-range distance and angle information for atoms located up to 40 Å from the paramagnetic center.[14] The determination of the complete structure with high precision exclusively from paramagnetic experiments, however, would require an excessive number of experiments to conjugate paramagnetic tags at different positions on the molecular surface to collect structural information covering the whole molecule. In practice, it is thus necessary for *de novo* structure determination to integrate multiple NMR data including NOEs, chemical shifts, PREs, PCSs, and RDCs.

Meanwhile, the visualization of the conformational distribution in the presence of large motions requires an ensemble structure calculation considering multiple states rather than a single conformation. Hence, we employed the multistate structure calculation method implemented into the program CYANA, which was originally applied to eNOE data of the protein GB1.[12] Based on the original algorithm, we here expand this method to other long-range experimental data, in particular for handling PCS data. The PCS $\Delta\chi$ tensors are determined iteratively based on intermediate structure ensembles during the calculation. To salvage NOEs that were not found by the conventional method due to large dynamics, the automated NOE assignment[15] was also performed repeatedly each time when the ensemble structures were updated. For systems with a large conformational distribution, these improvements for the multistate calculation are expected to be particularly effective.

As a model system for the multistate structure determination with multiple NMR data sets, we selected yeast ubiquitin hydrolase 1 (YUH1), which is composed of 236 residues with a molecular mass of 26.4 kDa. It belongs to the ubiquitin C-terminal hydrolases (UCHs) family of deubiquitinating enzymes with a function to detach small peptides or chemical adducts from the C-terminus of ubiquitin.[16,17] UCHs mainly contribute to the maintenance of the homeostatic equilibrium of ubiquitin level in eukaryotic cells by recycling ubiquitin after the proteasomal degradation in cell systems.[18] Since the primary sequence of ubiquitin is highly conserved in eukaryotes from yeast to human, the enzymatic processes of ubiquitination and deubiquitination must be similar. Despite numerous studies for UCHs, however, the molecular mechanism of ubiquitin recognition by UCH remains a fundamental question in molecular biology. The crystal structure of the YUH1 complex with ubiquitin aldehyde (Ubal)[19] demonstrates that the binding surface is divided primarily into two regions, one surrounding the enzymatic active site and the other interacting with the globular domain of ubiquitin (Figure S1A). Ubiquitin comprises a globular domain and a flexible C-terminus that anchors to other proteins during ubiquitination. The interaction surface of YUH1 with the globular domain of ubiquitin is presumably needed for the enzymatic reaction by tightly holding the ubiquitin domain in place. It is known that the active site of YUH1 consists of the cysteine nucleophile (Cys90), an adjacent histidine (His166), and an aspartate (Asp181).[19] The region surrounding the active site contains a loop which is referred to as the crossover loop (147−163) and the N-terminus (1−14; henceforth referred to as 'the gating lid' due to its location and its addition role elucidated in this study) of YUH1, forming a hole where the C-terminus of Ubal is entirely embedded, probably for the suppression of its flexibility (Figure S1A). In there, the ubiquitin C-terminus and the YUH1 N-terminus (gating lid) pass in parallel through the crossover loop, resulting in a tight packing of the hole. This observation raises the additional question as to how YUH1 efficiently and quickly incorporates the C-terminus of ubiquitin into the deep hole, catalyzes the hydrolysis at the optimal position, and releases it for the next cycle of the reaction. The configuration of the active site is well conserved among the UCH family,[20−23] indicating that this unique structural feature is indispensable for its enzymatic activity. Navarro et al. propose that the crossover loop restricts or filters the size of adducts of ubiquitin.[24] Two structural studies of ubiquitin carboxyl-terminal hydrolase isozyme L3 (UCHL3), which is the closest homologous human protein to YUH1, in its free state and in complex with ubiquitin demonstrate that the atomic coordinates of the crossover loop could be determined only in the complex, but not in the free state, suggesting that the crossover loop is highly flexible in the unbound form of UCHL3,[25] suggesting that the crossover loop is fairly flexible in the free state. This flexibility probably enables the efficient insertion of the ubiquitin C-terminus into the deep hole at the active site. Indeed, in our previous solution NMR study of free YUH1, the $^{1}H-^{15}N$ correlation cross-peaks in the 2D HSQC spectrum were distinctly strong for this region, and very few medium/long-range NOEs were detected in the ^{15}N-separated NOESY spectrum.[26] On the other hand, temperature factors are relatively low for this region in the crystal structure of the complex YUH1 with Ubal, implying that the crossover loop gets rigid through the interaction with ubiquitin (Figure S1B). Considering that the flexible property of YUH1 is presumably susceptible to the surrounding environment as described above, it is essential to elucidate its dynamics and structural distribution in the solution state.

In this article, we investigate the 3D structure of free YUH1 and its dynamics in solution by multistate structure determination using multiple types of NMR data sets. By integrating different types of spatial information derived from these data sets, the resulting ensemble structure becomes more reliable and representative. Visualizing the ensemble structures of YUH1 by this method demonstrates large dynamics not only in the crossover loop but also in the N-terminus (gating lid) of YUH1. The latter raises a further question as to whether these dynamics correlate with a molecular function. Hence, based on the conformational distributions and enzymatic activity measurements of several YUH1 mutants, we propose

https://doi.org/10.1021/jacs.5c06502
J. Am. Chem. Soc. 2025, 147, 29884−29894

an additional role of the N-terminus and discuss the molecular mechanism of ubiquitin hydrolysis by YUH1.

RESULTS

Protein Structure and Dynamics Analysis by Conventional Approaches. The backbone $^{1}H^{N}$, ^{15}N, $^{13}C^{\alpha}$, $^{13}C'$ and side chain $^{13}C^{\beta}$ resonances of free YUH1 have already been assigned in our previous study.[26] By analyzing 3D triple-resonance NMR spectra as well as 3D ^{15}N- and ^{13}C-separated NOESY spectra, we now assigned approximately 95% of H^{α}, and 98% of H^{β} resonances of YUH1 (Figure 1A and S2).

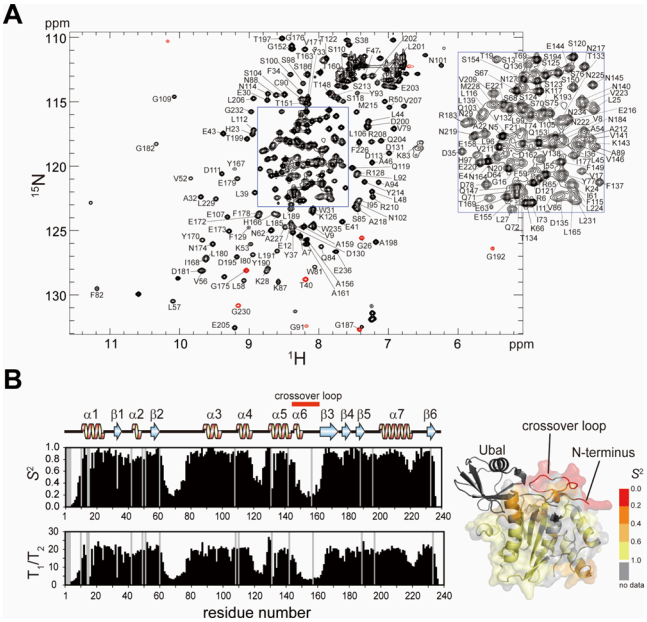

Figure 1. Backbone resonance assignments and dynamics of YUH1. **A** 2D $^{1}H-^{15}N$ HSQC spectrum and backbone resonance assignments of YUH1. The center area surrounded by the blue frame is separately shown on the right top. Positive and negative (aliased on the ^{15}N axis) signals are color-coded in black and red, respectively. **B** Generalized order parameters (S^2) for the $^{15}N-^{1}H$ vector of each residue calculated from T_1/T_2 relaxation and heteronuclear $\{^{1}H\}$-^{15}N NOE measurements. The S^2 values are mapped on the crystal structure of the YUH1-Ubal complex.

Methyl resonances were first classified into Ala, Ile, Leu, and Val by amino acid-selective labeling, and then 99% of the methyl $^{1}H-^{13}C$ resonances were assigned by analyzing 3D HC(C)H-TOCSY, ^{15}N- and ^{13}C-separated NOESY spectra (Figure S3). Similarly, amino-acid type classification for aromatic residues was performed by amino acid-selective labeling, and 89 out of 104 (86%) of the aromatic $^{1}H-^{13}C$ resonances were assigned by analyzing 3D ^{15}N- and ^{13}C-separated NOESY spectra. Using manual and automated NOE assignment implemented into the program CYANA,[15] overall 3605 distance restraints (including 1462 long-range) involving methyl and aromatic groups were assigned and used in the structure calculation. In addition, 288 dihedral angle restraints for ϕ and ψ angles were derived from backbone chemical shifts and restraints for 13 hydrogen bonds were collected by scalar-couplings ($^{3h}J_{N-C'}$) from a long-range HNCO experiment.[27]

We first performed a conventional structure calculation exclusively using distance and dihedral angle restraints from NOEs, hydrogen bonds, and chemical shifts. The resulting ensemble of 20 structures was well converged with an average backbone RMSD of 0.56 Å to the mean coordinates except for the N-terminus (gating lid; 1−14), the crossover loop (L9:149−164), and the "invisible" region in the YUH1-Ubal crystal structure (L5:63−77) (Figure S4A and Table S1). Except for these three regions, the global fold of free YUH1 was similar to that of YUH1 in the YUH1-Ubal crystal structure with a backbone RMSD of 2.85 Å (Figure S4C and Table S1). In contrast, the location of the gating lid was significantly different. In the YUH1-Ubal cocrystal, the gating lid passes through the crossover loop and lies besides the active center in the complex structure (Figure S4B), whereas it is oriented in the opposite direction pointing away from the crossover loop in the solution structure (Figure S4A, henceforth this conformation is referred to as the 'open conformation').

The number of long-range NOEs per residue in the above-mentioned three regions (gating lid, L5, and L9) is lower than elsewhere (Figure S5), suggesting large dynamics of these regions. Next, to quantify the dynamics, we measured the ^{15}N longitudinal (T_1) and transverse (T_2) relaxation times, and the steady-state heteronuclear $\{^{1}H\}$-^{15}N NOE (Figure S6). From these, the overall rotational correlation time τ_c, and effective correlation times τ_e and generalized order parameters S^2 for each $^{15}N-^{1}H$ vector were estimated by a Lipari-Szabo model-free analysis from the relaxation experiments (Figure 1B and S6). The τ_c from the model-free analysis was 14.3 ns, which is in good agreement with a rotational correlation time of 14.2 ns calculated by the Stokes−Einstein-Debye equation, validating this model-free analysis of the NMR relaxation data. The S^2 order parameters for the gating lid, L5, and L9 regions were below 0.6, demonstrating that they indeed possess large dynamics, while their temperature factors in the crystal structure of the complex in were relatively low (Figure S1B), indicating a well-defined structure. Interestingly, reports on free UCH-L3, which have approximately 60% sequence homology with YUH1 (Figure S7), have discussed that the crossover loop (L5) is quite flexible in the free state for efficient incorporation of the ubiquitin C-terminus into the active site.[21,29] However, these discussions were simply based on the fact that the crossover loop is invisible in the electron density of free UCH-L3. Consequently, our finding on YUH1 in solution is the first direct evidence for the large dynamics of the crossover loop.

Although ^{15}N-relaxation analysis reveals the dynamics of the gating lid, L5, and L9 regions of YUH1, the conformations of these regions found in the current single-state solution structure calculations were somewhat uncertain. The conformation of the gating lid differs strongly from that of the complex in the crystal (Figure S4B). As mentioned above, in the YUH1-Ubal crystal structure the N-terminal chain passes through the crossover loop and is located close to the active site Cys90. Comparing this with the gating lid location in the crystal structure of free UCH-L3, Johnston et al. proposed that the specificity of UCH to ubiquitin is enhanced by the steric obstruction of its N-terminus (gating lid) on the enzymatic active site.[19] Indeed, a side chain of the UCH-L3 N-terminus (gating lid) completely buries the catalytic cysteine nucleophile in the free structure. Since the current solution structure did not support this model, we performed PRE, PCS, and RDC experiments to obtain detailed long-range structural information on the relative orientation of the crossover loop and gating lid against the globular domain of YUH1 in solution.

https://doi.org/10.1021/jacs.5c06502
J. Am. Chem. Soc. 2025, 147, 29884−29894

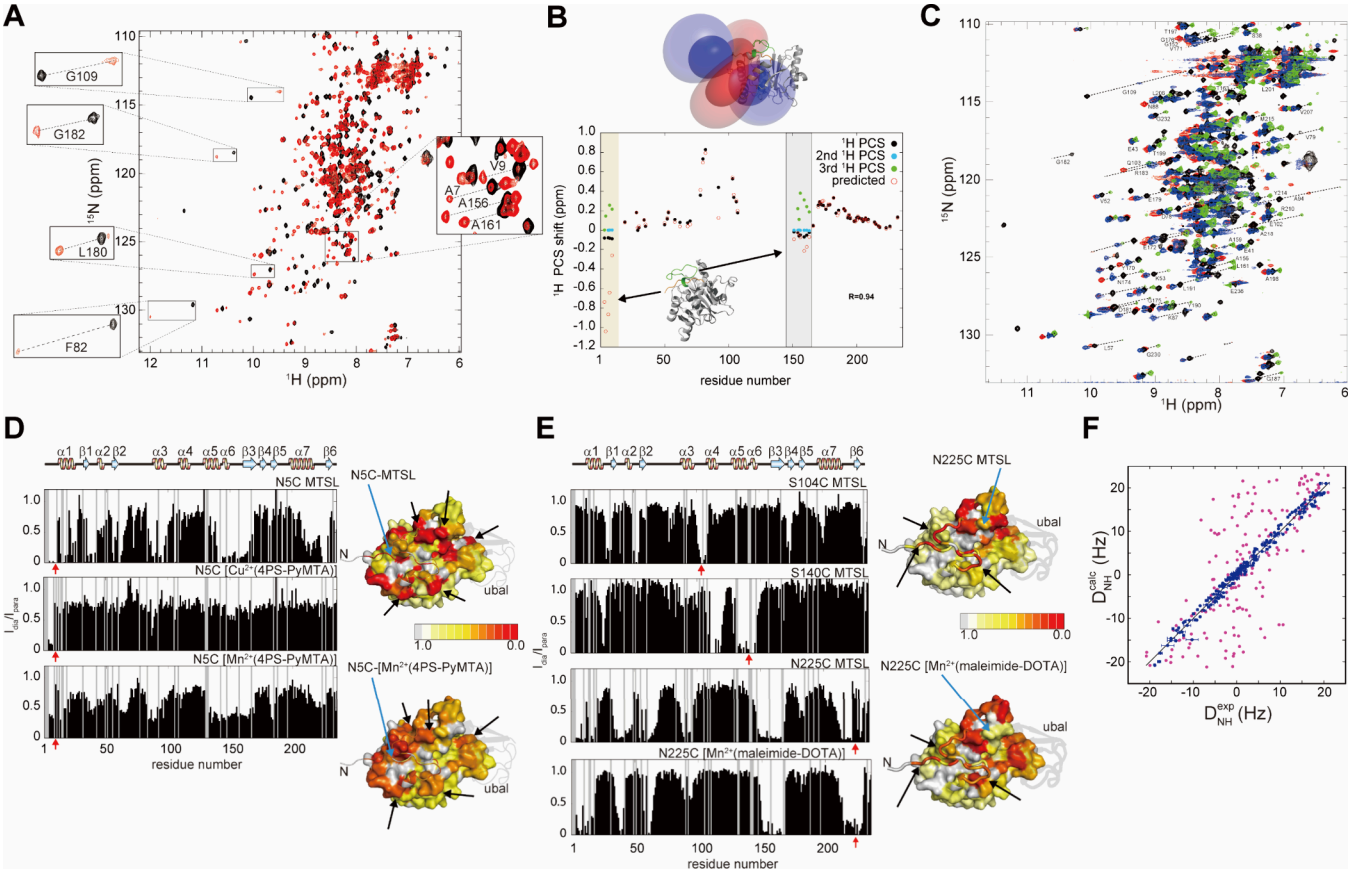

Figure 2. PRE, PCS and RDC measurements on YUH1. **A** ^{1}H−^{15}N HSQC spectra of YUH1(N140C) tagged with diamagnetic [Lu^{3+}(DOTA-M8-SPy)] (black) and paramagnetic [Dy^{3+}(DOTA-M8-SPy)] (red). Several representative cross peaks are shown in boxes and Figure S11. **B** Comparison of experimental PCSs (black; cyan and green for split cross peaks) from DOTA-M8-SPy for the free YUH1(N140C) with those predicted (red) from the YUH1 coordinates in the YUH1-Ubal crystal structure (PDB ID: 1CMX). The regions corresponding the gating lid (1−14) and crossover loop (L5) are shown in orange and gray strips, respectively. The $\Delta\chi$ tensors are represented by PCS isosurfaces, with positive and negative shifts shown in blue and red, respectively. **C** ^{1}H−^{15}N HSQC spectra of YUH1(N140C) tagged with DO3MA-3BrPy in the presence of diamagnetic Lu^{3+}(black) and paramagnetic Dy^{3+}(red), Tb^{3+} (blue), and Tm^{3+} (green). The crowding area and low intensity peaks are separately shown in Figure S11. **D** Ratios of peak heights between paramagnetic and diamagnetic samples (I_{para}/I_{dia}) of the free YUH1(N5C) tagged with MTSL, [Cu^{2+}(4PS-PyMTA)], and [Mn^{2+}(4PS-PyMTA)]. Red arrows indicate the spin-labeled positions. Residues are color-coded by I_{para}/I_{dia} ratios, as indicated in the color bar, on ribbon and surface models of the YUH1-Ubal crystal structure. The conformation for residues 1−5 that lack coordinates in the crystal structure was modeled by the CYANA regularize module.[28] Residues without data and Ubal are color-coded in gray and black, respectively. The black arrows indicate the regions that are far from the paramagnetic center but show strong PREs. **E** Ratios of peak heights between paramagnetic and diamagnetic samples (I_{para}/I_{dia}) of YUH1 S104C tagged with MTSL, S140C with MTSL, N225C with MTSL, and N225C with [Mn^{2+}(maleimide-DOTA)], color-coded as in panel D. **F** Correlation between observed RDCs and RDCs calculated on the basis of YUH1 structures computed by the conventional single-state method (red) or multistate structure calculation (blue). All spectra were recorded at 303 K and a magnetic field strength of 14.1 T.

PCS, PRE, RDC Experiments for Long-Range Structural Information. To conjugate paramagnetic tags to different sites on the protein surface, we produced four separate cysteine mutants. In all these mutants, the wild-type cysteine 90 was replaced with serine (C90S), and then one residue was replaced by a cysteine, N5C, S104C, N140C, and N225C (Figure S8). We observed no large perturbations of the ^{1}H−^{15}N-HSQC spectra between the wild type YUH1 and the four mutants except for the peaks of the replaced residues (Figure S9), indicating that the mutations did not alter the original fold of YUH1.

For PCS measurements, DOTA-M8-SPy[30] and DO3MA-3BrPy[31] were used depending on the reaction efficiencies at the cysteine mutation sites. Strong PCSs were observed in ^{1}H−^{15}N-HSQC spectra of the N140C mutant combined with DOTA-M8-SPy and DO3MA-3BrPy (Figure 2A-C, and Table S2), indicating sufficiently suppressed mobility of the tags and thereby accurate structural information. This analysis was conducted exclusively using the N140C mutant. We confirmed that these paramagnetic tags did not significantly affect the overall protein structure, as shown by the similarity of ^{15}N-HSQC spectra with and without the tags, except for residues near the labeling sites (Figure S10). In addition, because the line widths of the signals were not notably altered, we also concluded that the tag incorporations did not significantly affect the protein dynamics. The paramagnetic Dy^{3+} ion yielded single shifted ^{1}H−^{15}N correlation cross peaks for most of the affected residues, demonstrating that multiple orientations of the paramagnetic tag itself did not occur in this experiment. In contrast, surprisingly, most cross peaks corresponding to the gating lid and the crossover loop were split into two or three. For instance, in the ^{1}H−^{15}N HSQC spectrum of the N140C mutant combined with [Dy^{3+} (DOTA-M8-SPy)], Gly3 and Val9 showed cross peaks split into three,

https://doi.org/10.1021/jacs.5c06502
J. Am. Chem. Soc. 2025, 147, 29884−29894

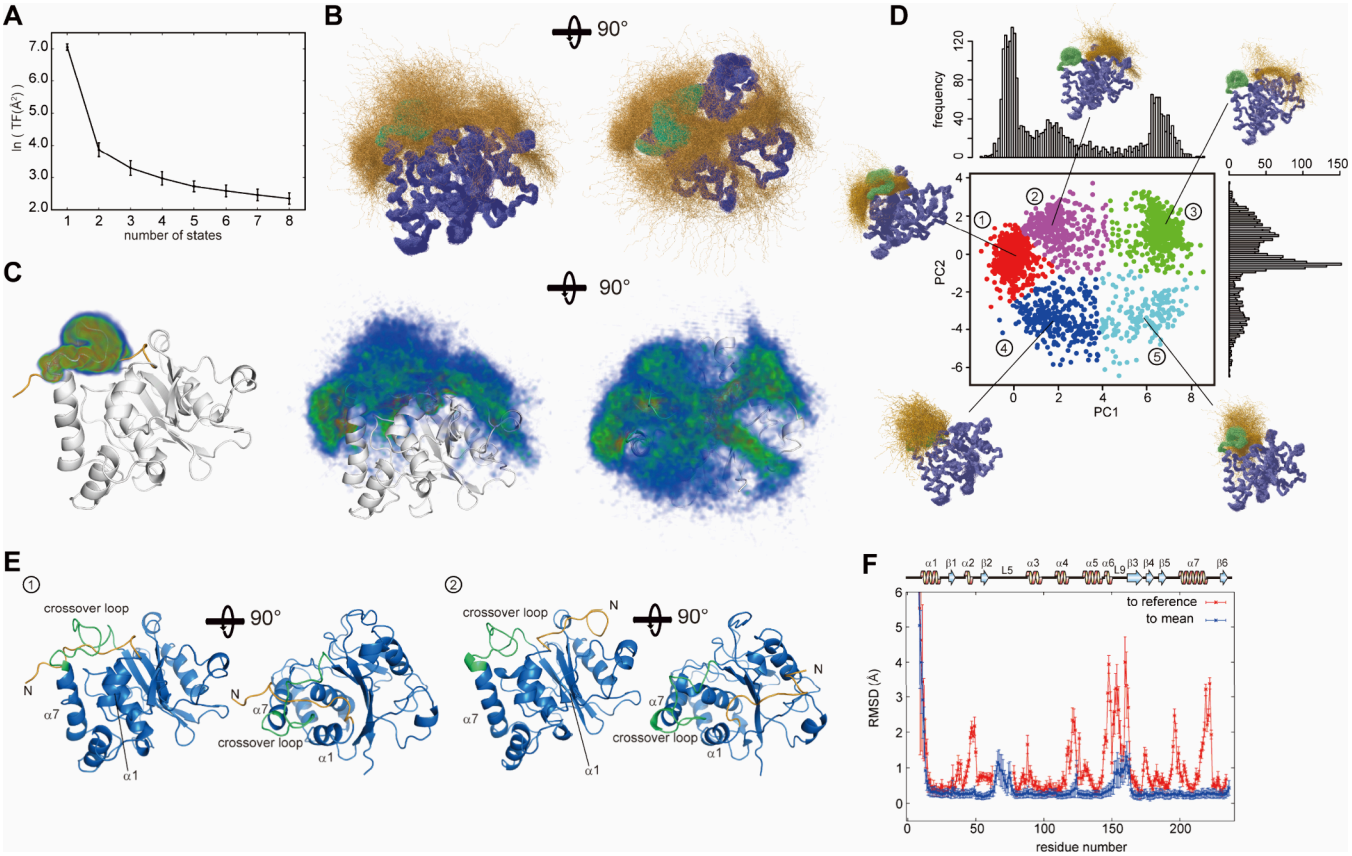

Figure 3. Ensemble structures of free YUH1. **A** Cross-validation tests highlighted by the CYANA target function per monomer which is the (weighted) sum of the squared violations of all experimental and steric conformational restraints. **B** 2500 conformers obtained by multistate structure calculation with a five-state model, showing the backbone atoms N, C^{α}, C'. The gating lid and the crossover loop are colored in orange and green, respectively. **C** Atomic probability density maps showing the conformational space sampled by this method for the crossover loop (left) and gating lid (center and right). **D** Distribution of 2500 conformers analyzed by principal component analysis (PCA). The horizontal and vertical axes show the first and second principal components, PC1 and PC2. The plot is classified by k-means clustering shown in different colors. Clusters are numbered in the order of their size. The histograms along the horizontal and vertical axes indicate the distributions on PC1 and PC2. **E** Representative conformations at the centers of the largest and second largest clusters in **D**, color-coded as in **B**. Ribbon models are representative conformations at the cluster centers. **F** RMSD per residue and its standard deviation for the 2500 conformations, computed for C^{α} to the mean structure (blue) and the crystal structure of YUH1-Ubal (red).

and Ala7, Ala156, Ala159, and Ala161 yielded cross peaks split into two. Figure 2B compares observed PCS values with those predicted from the YUH1 coordinates in the YUH1-Ubal cocrystal. The PCSs for the residues in the gating lid and the crossover loop are significantly different from the predicted values, whereas those for the rest of the residues show a good match. These results indicate that the gating lid and the crossover loop possess multiple conformations, each of which is different from that in the YUH1-Ubal crystal. Exchange between these conformations is slow on the NMR time scale, suggesting the presence of ~ msec dynamics.

To validate the split PCSs, we repeated the experiments by employing DO3MA-3BrPy with several lanthanoid ions, Dy^{3+}, Tb^{3+}, and Tm^{3+}, which are expected to provide various PCS effects due to their different paramagnetic properties. As expected, the resulting spectra exhibited similar doubled or tripled peaks but with different PCS values, again mostly for the residues in the gating lid and the crossover loop (Figure 2C and S11).

For PRE measurements, 4PS-PyMTA,[32] maleimide-DOTA,[33] and MTSL[34] were used as the paramagnetic probes by conjugating them to substituted cysteine residues through thioether or disulfide bonds. Strong PREs were observed for the N5C, S104C, N140C, and N225C mutants conjugated with MTSL, N225C with [Mn^{2+}(maleimide-DOTA)], and N5C with 4PS-PyMTA. We expected that the PRE-experiments on the N5C mutant, in which the paramagnetic tag is conjugated directly to the gating lid would validate or refine the gating lid conformations in solution. However, surprisingly, strong PREs were observed not only in the region surrounding the gating lid in the YUH1-Ubal crystal structure but also far away from it (Figure 2D). For instance, strong PREs by the MTSL and [Cu^{2+}(4PS-PyMTA)] tags at N5C were observed in the region 13−18, 35−42, 60−64, 97−99, 152−155, 164−169, and 224−227 which are more than 20 Å distant from Asn5 in the crystal structure. This result indicates that the gating lid does not always stay at one particular site seen in the crystal structure but instead dynamically samples different positions. Note that the spatial motion of the gating lid must be large-scale, since the gating lid first needs to exit from the tunnel formed by the crossover loop in order to approach the regions of residues 13−18, 35−42, 60−64, and 224−227. Similar behavior was also found in the PRE-experiment with MTSL-attached N225C (Figure 2E). In the complex structure, Arg6 in the gating lid is located over 25 Å away from Asn225, and Glu4 (missing its coordinates in the complex) would be

https://doi.org/10.1021/jacs.5c06502
J. Am. Chem. Soc. 2025, 147, 29884−29894

even further away than Arg6. Nonetheless, strong PREs were observed for residue 4−8. These results also suggest that the gating lid does not stay at the position in the YUH1-Ubal crystal structure but approaches the site of Asn225 for a certain period.

N−H^N RDCs were obtained by aligning with phage pf1 and measuring 2D ^{15}N−^{1}H IPAP HSQC[35] for the isotropic and aligned samples. We first calculated the alignment tensor and predicted RDCs based on the YUH1 coordinates in the YUH1-Ubal cocrystal. Just as for the results of the PCSs and PREs, the experimental data was not entirely consistent with those from the complex (Figure 2F), which further supports the hypothesis that the solution structure in the free state is quite different from the one in the YUH1-Ubal crystal.

Multistate Structure Calculation. The data from PCSs, PREs, and RDCs for free YUH1 in solution was not compatible with a single-conformation model, particularly for the gating lid and the crossover loop due to their large dynamic motions. Thus, we adopted multistate structure calculation using the program CYANA to analyze simultaneously several NMR data sets, including NOEs, chemical shifts, PREs, PCSs, and RDCs. Based on the original algorithm,[12] we expanded this method for handling other long-range experimental data, in particular PCS data. The PCS $\Delta\chi$ tensors were determined iteratively based on an intermediate structure ensemble during the calculation (Table S1). In the initial step, NOE assignments derived from the conventional single-state CYANA calculation were used. Following the generation of the first multistate ensemble, additional automated NOE assignments were performed using network-anchoring and constraint combination,[15] referring to intermediate ensemble conformations. This iterative process enabled the recovery of additional NOEs, especially in high-mobility regions such as the gating lid and the crossover loop (Figure S12). This procedure was repeated until the number of NOE assignments no longer changed substantially. A cross-validation test was performed to determine the optimal number of the conformational states (Figure 3A). The results show that increasing the number of conformations progressively decreases the CYANA target function. This trend continued up to eight, which was the maximum number of states addressed in this study. To assess statistical significance, a pairwise *t*-test was conducted based on the mean and standard deviation of the target functions for each number of states. The resulting *p*-values for comparisons between models with *i* and *i* + 1 states were 2.2×10^{-16}, 1.9×10^{-5}, 3.9×10^{-3}, 0.011, 0.10, 0.14, and 0.18, for *i* = 1−7, respectively. Assuming a threshold of 5% for statistical significance, the improvement beyond the five-state model was not significant. This indicates that the five-state model most appropriately fulfils the experimental data without overfitting (Figures 3A and S13, and Table S3). Compared with the single-state structures from the conventional method, the five-state ensemble conformations are in good agreement with the RDC data. The correlation between the back-calculated and experimental RDCs improved dramatically over the single-state structure (Figure 2F).

Except for the gating lid, the crossover loop (L9), and invisible regions in the YUH1-Ubal crystal structure (L5), the global fold of the five-state ensemble structures was very similar to the complex with a backbone RMSD of 2.02 Å for residues 15−62, 78−148, and 165−236 (Figure 3B-D and 4A). Meanwhile, the gating lid and crossover loop spread out over an extensive region in conformational space, but their

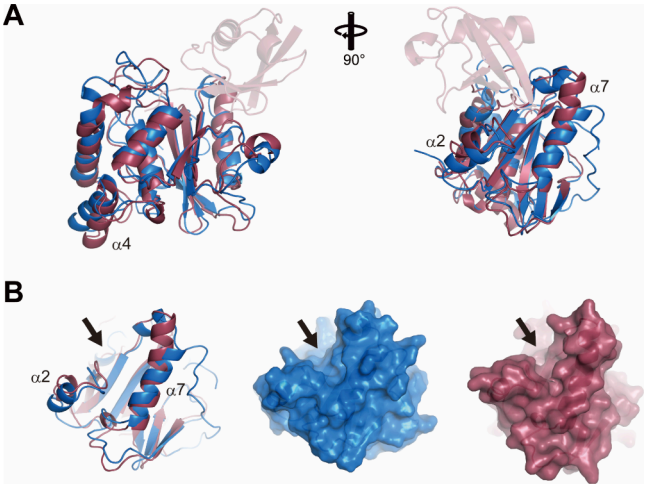

Figure 4. Comparison of the free YUH1 structure with the YUH1-Ubal complex. **A** Superposition of the free YUH1 structure at the center of the largest cluster (light blue), and the complex (dark red). Ubal is shown in dim red. **B** Interaction surface with the ubiquitin globular domain of free YUH1 (light blue) and the complex (dark red). The arrows show the direction of the ubiquitin binding.

structures are not entirely random. To analyze the structural distribution based on representative variances of 3D coordinates, we performed principal component analysis (PCA) on the atomic coordinates of C^{α} atoms and k-means clustering with the assumption of the existence of five clusters in the plane spanned by the first and second principal components (PC1 and PC2) (Figure 3D).[36,37] The largest cluster was the most compact distribution on the PC1 and PC2 plane. 1059 out of all 2500 conformers (∼42%) belong to this cluster and are very similar to the YUH1-Ubal crystal structure with an average backbone RMSD of 2.26 Å for all residues present in the crystal structure, 6−62 and 78−234. The structures of the first cluster are in the closed form in which the gating lid passes through the crossover loop and orients toward the active center's side (Figure 3E, left panel). This suggests that the two regions are extraordinarily flexible but still mostly adopt as the closed form even in the free state. All clusters, except the first and fifth, comprised conformers in which the gating lid does not pass through the crossover loop and is oriented in different directions against the crossover loop. The second-largest cluster (∼23%) predominantly consists of conformations in which the gating lid is located at the binding site for the ubiquitin globular domain (Figure 3E). The binding site constitutes a large groove, into which the gating lid fits well. The third and fourth cluster are roughly in between the first and second, in that the gating lid is rotated approximately 90 deg away from its positions in the first and second clusters. They might be intermediate conformations in the equilibrium between the first (closed) and second (open) forms. The structures in the fifth cluster contained similar gating lid orientations as in the YUH1-Ubal crystal structure but consisted of two different forms where the gating lid passes over and under the crossover loop, respectively. Given the observation of multiple peaks in the PCS data and the nonuniform PRE effects upon spin labeling of the gating lid, these results support that the protein interconverts between several distinct conformational states.

The binding surface with the ubiquitin globular domain is well converged in all ensemble structures of free YUH1 and

https://doi.org/10.1021/jacs.5c06502
J. Am. Chem. Soc. 2025, 147, 29884−29894

similar to the complex, where two α-helices (α2 and α7) constitute the large groove (Figure 4B). Meanwhile, the α7 helix in the free state structure is tilted slightly in the direction of widening the groove. Considering that the order parameters are relatively low at the end of this helix (Figure 1B), the free structure possesses a flexible and wider groove than that of the complex, presumably to facilitate the access of ubiquitin. Consequently, a conformational change is likely to occur when YUH1 binds with ubiquitin. The L5 loop, which was invisible in the YUH1-Uba1 crystal structure, is not well converged compared with other regions in the free solution state (Figure 3F).

Specific Interactions of the Gating Lid of YUH1 with Ubiquitin. The NMR experiments and multistate structure calculation elucidated that the gating lid and crossover loop possess large conformational variability. While the large dynamics of the crossover loop is in line with previous reports on homologous proteins such as UCH-L3,[19] it has never been discussed that the gating lid passes transiently through and slips out of the crossover loop, resulting in the extensive conformational distribution of these regions. This result proposed a new hypothesis that its dynamics may correlate with an unknown function of the YUH1 gating lid. To elucidate the functional significance of this dynamics using a simpler model, we first performed an NMR titration experiment of a short peptide from the YUH1 N-terminus (1−10) [henceforth referred to as YUH1(1−10)] with ubiquitin. It was expected that the titration of YUH1(1−10) with ubiquitin would reveal an interaction between the YUH1 gating lid and ubiquitin. Increasing the peptide ratio against ubiquitin, chemical shift perturbations of several peaks were observed (Figure 5A and B). Surprisingly, the most significant chemical shift changes were observed not only for the C-terminus but also the center of the ubiquitin globular domain. In the crystal structure of the YUH1-Ubal complex the YUH1 gating lid is close and parallel to the ubiquitin C-terminus but rather far from the center of the ubiquitin globular domain (Figure S1). Large chemical shift differences cluster around the β-strands of ubiquitin, demonstrating that the gating lid of YUH1 specifically interacts with ubiquitin in a different orientation from the complex structure. The region showing large chemical shift perturbations is charged positively and forms a shallow groove on the surface of ubiquitin (Figure 5C). Considering that the YUH1 gating lid is negatively charged, it may bind to this groove primarily by electrostatic interactions. The dissociation constant calculated from the chemical shift perturbations was approximately 180 μM. Comparing this to the dissociation constant of the YUH1-(C90S) mutant with ubiquitin that was reported as 43 nM,[38] the affinity of YUH1(1−10) to ubiquitin is over 1000 times lower, suggesting that the interaction of the gating lid with ubiquitin might be transient.

Hydrolysis Activity of YUH1 and the Role of the Gating Lid. The multistate structure calculation showed that the gating lid possesses extraordinarily large dynamics but not an entirely random structure. To elucidate the correlation between the large-scale dynamics and ubiquitin-specific interaction of the gating lid with the YUH1 hydrolysis activity, we produced two mutants, an N-terminal deletion [henceforth referred to as YUH1(11−236)] and the V9P mutant. The replacement of valine 9, located near the N-terminus, to proline was expected to suppress the dynamics of the gating lid due to its rigidifying effect on the protein backbone. The T_1/T_2

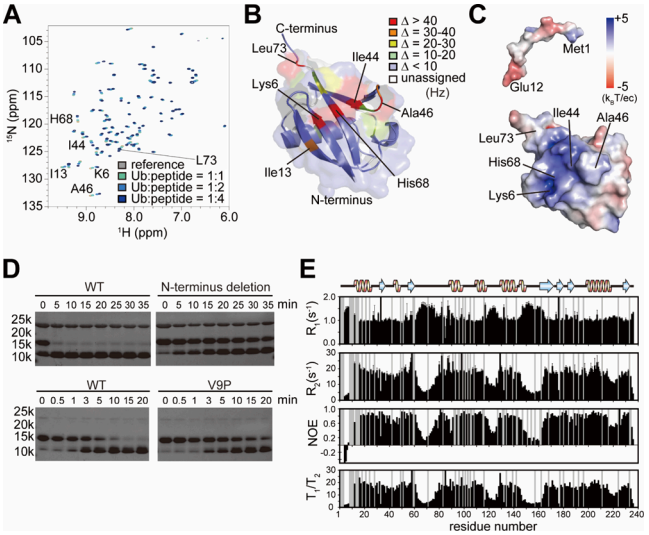

Figure 5. Functional assay of the YUH1 gating lid. **A** Overlays of 2D ^{1}H−^{15}N HSQC spectra from multipoint titrations of ^{15}N-ubiquitin with the unlabeled N-terminus peptide of YUH1 (residues 1−10). The color codes of ^{1}H−^{15}N correlation cross-peaks at each titration point, showing the molar ratio of ubiquitin:peptide, are as follows: gray (1:0); green(1:1); light blue (1:2); blue (1:4). **B** Chemical shift changes Δ for ubiquitin upon binding of the N-terminus peptide, YUH1(1−10), mapped on a ribbon and surface model of the crystal structure of ubiquitin (PDB ID: 1UBQ). **C** Electrostatic potential for the N-terminal peptide and ubiquitin indicated by colored surface models. **D** YUH1 hydrolysis activity on Ub-Rec33 fusion protein. Reaction samples were collected at the given time points and subjected to SDS-PAGE electrophoresis for wild type (top and bottom left), the gating lid deletion mutant (top right) of YUH1, and the V9P mutant (bottom right). The reactions shown in the top and bottom panels were conducted at 25 and 20 °C, respectively. YUH1, Ub-Rec33 fusion protein, and cleaved Ub (in addition to a His_{10} tag at the Ub-Rec33 N-terminus) appear as a band at about 26, 15, and 11 kDa, respectively. Cleaved Rec33 is invisible on these electrophoresis gels because of its small size of 4 kDa. **E** $T_1(R_1)$, $T_2(R_2)$, and $\{^{1}H\}$-^{15}N NOE for backbone ^{15}N resonances of YUH1(V9P). Residues without data are shown in gray. Error bars shown in the R_1 and R_2 graph ware calculated using bootstrap method with 1000 cycles.

relaxation for the V9P mutant showed slightly longer T_2 relaxation times (larger R_2) for the gating lid than for the wild type (Figure 1B, 5E, S6), indicating that the V9P mutant indeed influences the gating lid dynamics. It is considered that the chemical exchange contribution to the T_2 relaxation time is suppressed by the V9P mutant. On the basis of this physical property of the V9P mutant, the deubiquitination activities of both mutants as well as the wild type were evaluated at 25 °C by employing a ubiquitin fused with its C-terminus to the N-terminal 33 residues of *E. coli* RecA (Rec33) (henceforth referred to as Ub-Rec33). The SDS−PAGE analysis of the activity for the wild type YUH1 showed that the ubiquitin part was observed at the expected molecular size, showing that Ub-RecA33 was hydrolyzed precisely (Figure 5D). In comparison with the wild type, YUH1(11−236) shows dramatically reduced hydrolysis activity. It did not completely cleave Ub-Rec33 even after 35 min while the wild type did it almost within 5 min, indicating that the gating lid significantly contributes to the enzymatic activity of YUH1. In contrast, under the same reaction conditions, the V9P mutant cleaved Ub-Rec33 as fast as the wild type (Figure S14). However, when repeating the experiments with a 20 times lower

https://doi.org/10.1021/jacs.5c06502
J. Am. Chem. Soc. 2025, 147, 29884−29894

concentration of YUH1 and at a lower temperature of 20 °C, the V9P mutant failed to completely hydrolyze Ub-Rec33 even after 20 min, while the wild type achieved it within 15 min. This reduction of the enzymatic activity of YUH1 might be attributed to the change in the gating lid dynamics, which was demonstrated by the T_1/T_2 relaxation experiment. These biochemical analyses of YUH1(11−236) and the V9P mutant suggest that the gating lid and its dynamics are essential for the efficiency of the YUH1 function.

Multiple Conformations of the YUH1-Ubiquitin Complex. The multistate structure determination and titration experiments of YUH1(1−10) with ubiquitin demonstrated that free YUH1 possesses multiple conformations and transiently interacts with different sites of ubiquitin. It indicates that the interaction of YUH1 with ubiquitin also includes multiple states. To investigate the binding states between YUH1 and ubiquitin, we recorded ^{1}H−^{15}N TROSY spectra for ^{2}H, ^{15}N-ubiquitin in the presence of nonlabeled YUH1 at a low temperature (283 K), which slows down molecular motions. Notably, two resonances were observed for K11, I13, T15, I36, D39, A46, K48, Q49, L67, H68, and V70 of ubiquitin (Figure 6A), while only one resonance was observed for these residues in the spectra of ^{2}H,^{15}N-Ubal-unlabeled YUH1 complex. One of the split peaks in the ubiquitin-YUH1 complex was identical with that of the Ubal-YUH1 complex. These residues correspond to the interface of the YUH1-complex (Figure 6B), suggesting that the interaction between ubiquitin and YUH1 is also composed of multiple-states in addition to the conformation observed in the Ubal-YUH complex.

DISCUSSION

The multistate structure calculation with multiple NMR data sets presented here reveals large dynamics of the gating lid and the crossover loop of YUH1. In particular, the extensive motions of the gating lid first elucidated by this method allow us to find its potential functional significance. Based on the conformational ensemble, dynamics and interaction analysis by NMR, and biochemical evidence for the hydrolysis activity of the YUH1 mutants, we propose a new recognition mechanism of YUH1 with ubiquitin (Figure 7). In the initiation of its reaction cycle, the free YUH1 exists in a largely fluctuating state for the regions surrounding the active site, the gating lid and crossover loop. The gating lid of YUH1 is predominantly in equilibrium between two conformations, the closed form passing it through the crossover loop and the open form spreading widely by slipping it out of the loop. The titration experiment of ubiquitin with YUH1(1−10) demonstrates that the flexible gating lid specifically interacts with both the β-sheet in the globular domain and the C-terminus of ubiquitin. Truncation of the N-terminus in YUH1(11−236) dramatically reduces the enzymatic activity, and the V9P mutant shows moderately reduced activity. Longer T_2 relaxation times for the gating lid in the V9P mutant indicate that a modulation of molecular motion for the gating lid occurs, which is presumably responsible for the reduced enzymatic activity. An earlier structural study of free UCH-L3 suggested that the function of its N-terminus is to prohibit nonspecific enzymatic activity by covering the active center residue Cys90.[19] However, the reduction of enzymatic activity by modifications on the YUH1 gating lid indicates that it at least does not work for suppressing the nonspecific catalytic cysteine nucleophile but rather enables its efficient reaction. Considering that the gating lid interacts not only with the ubiquitin C-terminus but

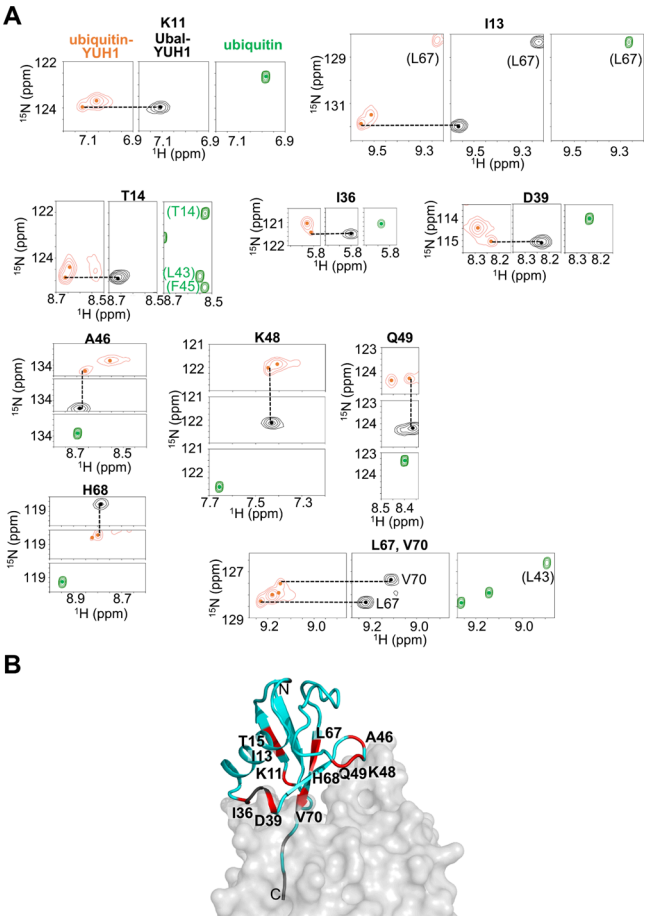

Figure 6. Multiple conformations of the YUH1-ubiquitin complex. **A** 2D ^{1}H−^{15}N TROSY spectrum of 0.85 mM ^{2}H, ^{15}N-ubiquitin with 1.45 mM unlabeled YUH1 (orange) and 0.5 mM [^{2}H, ^{15}N] Ubal-unlabeled YUH1 complex (black). Only the regions with K11, I13, T15, I36, D39, A46, K48, Q49, L67, H68, and V70 resonances are shown, and the center of the peaks are indicated with dots. Dashed lines represent the ^{1}H or ^{15}N chemical shifts of the resonances of Ubal-YUH. Full spectra are shown in Figure S15. **B** Mapping of the residues (red) on Ubal that exhibited two resonances in the spectrum of the YUH1-Ubal complex (PDB ID: 1CMX). The residues with one resonance are color-coded in light blue, and the ones with no data, proline residues, or probably due to the line broadening, are colored in gray. YUH1 and Ubal are shown in the surface and ribbon representation, respectively.

also its globular domain, we propose a unique function of the gating lid that might capture a free ubiquitin and guide it to the binding and enzymatic active site. Based on the crystal structure of the YUH1-Ubal complex, the binding surface comprises roughly two regions, one surrounding the enzymatic active site with the C-terminus of ubiquitin (site A) and the other interacting with the ubiquitin globular domain (site B). Since site B is composed of an open groove, its interaction is presumably more straightforward and faster than that of site A forming a narrow and deep hole. Thus, we assume that the initial step of the reaction is that the YUH1 gating lid captures the free ubiquitin and introduces it to site B. The ubiquitin-binding occurs as an induced fit where the site B groove narrows by the slight tilt of the α7 helix. During this process, the YUH1 gating lid would detach from the interaction with the β-sheet of ubiquitin, move toward the active site and pass through the crossover loop. The ability for the gating lid to

https://doi.org/10.1021/jacs.5c06502
J. Am. Chem. Soc. 2025, 147, 29884−29894

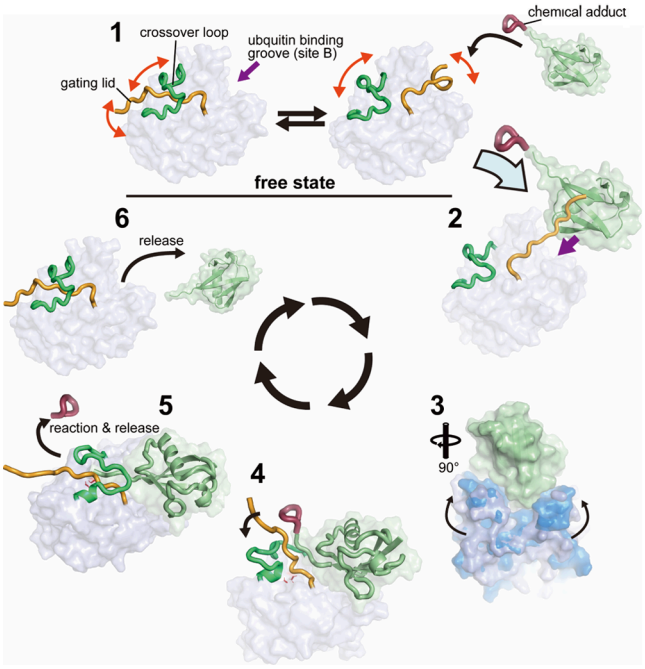

Figure 7. A proposed molecular recognition model for the ubiquitin C-terminal hydrolysis by YUH1. **1**) Free YUH1 is in the equilibrium state comprising both, the closed form with the gating lid passing through the crossover loop and the open form slipping the gating lid out of the loop. **2**) When ubiquitin is nearby, the YUH1 gating lid captures it as lariat by interacting with its globular domain. **3**) The ubiquitin globular domain binds at the site B of YUH1, and a conformational change primarily in helix α7 occurs. **4**) The gating lid dissociates from the ubiquitin globular domain and moves toward the enzymatic active center passing through the crossover loop along with the ubiquitin C-terminus. **5**) The crossover loop and gating lid of YUH1 anchor the ubiquitin C-terminus and hydrolyze a chemical adduct attached to the ubiquitin C-terminus. **6**) YUH1 releases ubiquitin and returns to the equilibrium state.

bind both with the ubiquitin C-terminus and the globular domain (Figure 5C) indicates that the location shift of the YUH1 gating lid might occur together with the introduction of the ubiquitin C-terminus into the active site. Hence, the YUH1 gating lid might work as a guide of the ubiquitin C-terminus to the catalytic center. Considering that the temperature factors of the crystal structure of the YUH1-Ubal complex are relatively low in the active site, this area would be fixed after the passing process of the YUH1 gating lid and ubiquitin C-terminus through the crossover loop for the sake of an efficient and specific reaction. Finally, the enzyme performs the cleavage of the chemical adduct from the ubiquitin C-terminus. After the reaction, YUH1 releases ubiquitin and returns to the equilibrium between the open and closed states again. Observation of two sets of resonances for the YUH1-ubiquitin complex (Figure 6) provides evidence for the above-described multistep interaction, and it is tempting to speculate that the split resonances observed for the ubiquitin-YUH complex may correspond to the states before and after the passing process of the gating lid, or multiple binding sites of ubiquitin with the gating lid. The results of this study and previous crystal structures clearly demonstrate that the gating lid of YUH1 passes through the crossover loop in certain structural states of free YUH1 or when ubiquitin is conjugated to a minimal substrate such as Ubal. This observation suggests a possible role for the gating lid and crossover loop in substrate size discrimination. On the other hand, in the case of UCHL3, substrate selectivity has been shown to depend not only on size but also thermal stability.[24] In such cases, alternative substrate recognition mechanisms may be involved. Further structural studies, including multistate structure calculations of YUH1 in complex with larger and partially disordered substrates, will be necessary to explore these possibilities.

Using YUH1 as a model system, we demonstrated in this study that multistate structure determination with multiple NMR data sets can be employed for general protein structure analysis and opens an avenue toward a comprehensive spatial description of 3D structures and the dynamics of biomacromolecules. Structure determination by X-ray crystallography may not allow observation of widespread conformational distributions such as the large motion of the YUH1 gating lid due to the suppression of dynamics in a crystal. It is crucial to observe the flexible regions in solution or under near-physiological conditions because of their susceptibility for their surrounding environment. In this study, spin labels were introduced into the protein to validate its large conformational flexibility and to obtain direct structural information. Although the possibility that the spin labels affect the protein's structure and dynamics cannot be entirely excluded, we believe such effects are minimal. This interpretation is supported by the ^{1}H-^{15}N HSQC spectra of the tagged proteins in the diamagnetic state, which showed that chemical shift perturbations and line broadening were negligible for most residues, except a few near the labeling site (Figure S10). Nonetheless, further investigations that go beyond the scope of this manuscript will be required to evaluate this possibility. Therefore, complementary approaches such as CPMG relaxation dispersion[39] and CEST,[7] which do not involve chemical modification, may also be employed in the future to independently validate these findings. Combining NMR CPMG relaxation dispersion and CEST with our method, one can also quantify the low population of each visualized conformation at various time scales related to the dynamic behavior, which may not be possible even with cryo-electron microscopy. In this respect, NMR spectroscopy is better suited for such studies than the other methods.

Our results demonstrate that, in addition to the conventional structural information from NOEs and chemical shifts, the paramagnetic effects and RDCs are powerful tools to uncover the conformational distribution. Until recently, it was not straightforward to collect accurate paramagnetic effects, in particular due to the large conformational flexibility of the metal-binding tags themselves. However, recent progress on lanthanoid-binding tags encourages us to observe the paramagnetic effects accurately and easily. Hence, we believe that it is now possible to perform ensemble structure determinations of various biomolecules and uncover molecular interactions and functions based on comprehensive spatial description. Moreover, the current NMR methodologies allow us to measure biomolecules at atomic resolution even in living cells (in-cell NMR).[40,41] Expanding our method to in-cell NMR can be a further useful tool to elucidate the physiological importance of protein dynamics through structural biology.

■ ASSOCIATED CONTENT

Supporting Information

The Supporting Information is available free of charge at https://pubs.acs.org/doi/10.1021/jacs.5c06502.

https://doi.org/10.1021/jacs.5c06502
J. Am. Chem. Soc. 2025, 147, 29884−29894

Figures S1−S15, Tables S1−S3, Listing 1, Experimental Section (procedures of protein sample preparations, NMR measurements, computational data analysis), References (PDF)

AUTHOR INFORMATION

Corresponding Authors

Yutaka Ito − *Department of Chemistry, Graduate School of Science, Tokyo Metropolitan University, Hachioji, Tokyo 192-0397, Japan; International Graduate School of Arts and Sciences, Yokohama City University, Yokohama 230-0045, Japan*; Email: ito-yutaka@tmu.ac.jp

Teppei Ikeya − *Department of Chemistry, Graduate School of Science, Tokyo Metropolitan University, Hachioji, Tokyo 192-0397, Japan*; orcid.org/0000-0002-6721-3727; Email: tikeya@tmu.ac.jp

Authors

Mayu Okada − *Department of Chemistry, Graduate School of Science, Tokyo Metropolitan University, Hachioji, Tokyo 192-0397, Japan*

Yutaka Tateishi − *Department of Chemistry, Graduate School of Science, Tokyo Metropolitan University, Hachioji, Tokyo 192-0397, Japan*

Eri Nojiri − *International Graduate School of Arts and Sciences, Yokohama City University, Yokohama 230-0045, Japan*

Tsutomu Mikawa − *Department of Chemistry, Graduate School of Science, Tokyo Metropolitan University, Hachioji, Tokyo 192-0397, Japan; International Graduate School of Arts and Sciences, Yokohama City University, Yokohama 230-0045, Japan; RIKEN Center for Biosystems Dynamics Research, Yokohama 230-0045, Japan*; orcid.org/0000-0003-2325-5084

Sundaresan Rajesh − *International Graduate School of Arts and Sciences, Yokohama City University, Yokohama 230-0045, Japan*

Hiroki Ogasa − *Graduate School of Pharmaceutical Sciences, The University of Tokyo, Bunkyo-ku, Tokyo 113-0033, Japan*

Takumi Ueda − *Graduate School of Pharmaceutical Sciences, The University of Tokyo, Bunkyo-ku, Tokyo 113-0033, Japan; Graduate School of Pharmaceutical Sciences, The University of Osaka, Osaka 565-0871, Japan*

Hiromasa Yagi − *RIKEN Center for Biosystems Dynamics Research, Yokohama 230-0045, Japan*; orcid.org/0000-0001-8059-4440

Toshiyuki Kohno − *Department of Medical Informatics, Research and Development Center for Medical Education, Kitasato University School of Medicine, Sagamihara, Kanagawa 252-0374, Japan*

Takanori Kigawa − *RIKEN Center for Biosystems Dynamics Research, Yokohama 230-0045, Japan*; orcid.org/0000-0003-0146-9719

Ichio Shimada − *RIKEN Center for Biosystems Dynamics Research, Yokohama 230-0045, Japan; Graduate School of Pharmaceutical Sciences, The University of Tokyo, Bunkyo-ku, Tokyo 113-0033, Japan; Graduate School of Integrated Sciences for Life, Hiroshima University, Hiroshima 739-8528, Japan*; orcid.org/0000-0001-9864-3407

Peter Güntert − *Department of Chemistry, Graduate School of Science, Tokyo Metropolitan University, Hachioji, Tokyo 192-0397, Japan; Institute of Biophysical Chemistry, Center for Biomolecular Magnetic Resonance, Goethe University Frankfurt, Frankfurt am Main 60438, Germany; Institute for Molecular Physical Science, ETH Zürich, Zürich 8093, Switzerland*

Complete contact information is available at: https://pubs.acs.org/10.1021/jacs.5c06502

Author Contributions

‡Mayu Okada and Yutaka Tateishi contributed equally.

Notes

The authors declare no competing financial interest.

ACKNOWLEDGMENTS

The authors thank Dr. Tsutomu Terauchi (Taiyo Nippon Sanso Corp.) and Dr. Youhei Kawabata for the useful discussions on paramagnetic tags and NMR relaxation, respectively. We gratefully acknowledge financial support from the Funding Program for Core Research for Evolutional Science and Technology (CREST; JPMJCR13M3 to Y.I. and JPMJCR21E5 to T.I.) from the Japan Science and Technology Agency (JST), Grants-in-Aid for Scientific Research (JP15K06979 to T.I., JP19H05645 to Y.I., and JP20K06508 and JP23K05660 to P.G.) and Scientific Research on Innovative Areas (JP15H01645, JP16H00847, JP17H05887, and JP19H05773 to Y.I. and JP26102538, JP25120003, JP16H00779, and JP21K06114 to T.I.) from the Japan Society for the Promotion of Science (JSPS), Shimadzu foundation, and the Precise Measurement Technology Promotion Foundation. The NMR experiments were performed at the NMR Platform supported by the Ministry of Education, Culture, Sports, Science and Technology (MEXT) Program Grant Number JPMXS0450100021.

ABBREVIATIONS

YUH1, Yeast ubiquitin hydrolase 1; UCH, Ubiquitin C-terminal hydrolase; PCS, Pseudocontact shift; PRE, Paramagnetic relaxation enhancement; RDC, Residual dipolar coupling

REFERENCES

(1) Goh, C. S.; Milburn, D.; Gerstein, M. Conformational changes associated with protein-protein interactions. *Curr. Opin. Struct. Biol.* **2004**, *14* (1), 104−109.

(2) Wright, P. E.; Dyson, H. J. Intrinsically disordered proteins in cellular signalling and regulation. *Nat. Rev. Mol. Cell Biol.* **2015**, *16* (1), 18−29.

(3) Ikeya, T.; Güntert, P.; Ito, Y. Protein Structure Determination in Living Cells. *Int. J. Mol. Sci.* **2019**, *20* (10), 2442.

(4) Ito, Y.; Dötsch, V.; Shirakawa, M. *In-cell NMR Spectroscopy: From Molecular Sciences to Cell Biology*; The Royal Society of Chemistry, 2019. DOI: 10.1039/9781788013079.

(5) Korzhnev, D. M.; Kay, L. E. Probing invisible, low-populated States of protein molecules by relaxation dispersion NMR spectroscopy: an application to protein folding. *Acc. Chem. Res.* **2008**, *41* (3), 442−451.

(6) Fawzi, N. L.; Ying, J.; Ghirlando, R.; Torchia, D. A.; Clore, G. M. Atomic-resolution dynamics on the surface of amyloid-beta protofibrils probed by solution NMR. *Nature* **2011**, *480* (7376), 268−272.

(7) Vallurupalli, P.; Bouvignies, G.; Kay, L. E. Studying "invisible" excited protein states in slow exchange with a major state conformation. *J. Am. Chem. Soc.* **2012**, *134* (19), 8148−8161.

(8) Nodet, G.; Salmon, L.; Ozenne, V.; Meier, S.; Jensen, M. R.; Blackledge, M. Quantitative description of backbone conformational sampling of unfolded proteins at amino acid resolution from NMR

residual dipolar couplings. *J. Am. Chem. Soc.* **2009**, *131* (49), 17908−17918.
(9) Tang, C.; Schwieters, C. D.; Clore, G. M. Open-to-closed transition in apo maltose-binding protein observed by paramagnetic NMR. *Nature* **2007**, *449* (7165), 1078−1082.
(10) Liu, W.; Liu, X.; Zhu, G.; Lu, L.; Yang, D. A Method for Determining Structure Ensemble of Large Disordered Protein: Application to a Mechanosensing Protein. *J. Am. Chem. Soc.* **2018**, *140* (36), 11276−11285.
(11) Kooshapur, H.; Schwieters, C. D.; Tjandra, N. Conformational Ensemble of Disordered Proteins Probed by Solvent Paramagnetic Relaxation Enhancement (sPRE). *Angew. Chem., Int. Ed. Engl.* **2018**, *57* (41), 13519−13522.
(12) Vögeli, B.; Kazemi, S.; Güntert, P.; Riek, R. Spatial elucidation of motion in proteins by ensemble-based structure calculation using exact NOEs. *Nat. Struct. Mol. Biol.* **2012**, *19* (10), 1053−1057.
(13) Clore, G. M. Exploring sparsely populated states of macromolecules by diamagnetic and paramagnetic NMR relaxation. *Protein Sci.* **2011**, *20* (2), 229−246.
(14) Clore, G. M.; Iwahara, J. Theory, practice, and applications of paramagnetic relaxation enhancement for the characterization of transient low-population states of biological macromolecules and their complexes. *Chem. Rev.* **2009**, *109* (9), 4108−4139.
(15) Güntert, P.; Buchner, L. Combined automated NOE assignment and structure calculation with CYANA. *J. Biomol. NMR* **2015**, *62* (4), 453−471.
(16) Liu, C. C.; Miller, H. I.; Kohr, W. J.; Silber, J. I. Purification of a Ubiquitin Protein Peptidase from Yeast with Efficient Invitro Assays. *J. Biol. Chem.* **1989**, *264* (34), 20331−20338.
(17) Song, L.; Luo, Z. Q. Post-translational regulation of ubiquitin signaling. *J. Cell Biol.* **2019**, *218* (6), 1776−1786.
(18) Nijman, S. M.; Luna-Vargas, M. P.; Velds, A.; Brummelkamp, T. R.; Dirac, A. M.; Sixma, T. K.; Bernards, R. A genomic and functional inventory of deubiquitinating enzymes. *Cell* **2005**, *123* (5), 773−786.
(19) Johnston, S. C.; Riddle, S. M.; Cohen, R. E.; Hill, C. P. Structural basis for the specificity of ubiquitin C-terminal hydrolases. *EMBO J.* **1999**, *18* (14), 3877−3887.
(20) Das, C.; Hoang, Q. Q.; Kreinbring, C. A.; Luchansky, S. J.; Meray, R. K.; Ray, S. S.; Lansbury, P. T.; Ringe, D.; Petsko, G. A. Structural basis for conformational plasticity of the Parkinson's disease-associated ubiquitin hydrolase UCH-L1. *Proc. Natl. Acad. Sci. U S A* **2006**, *103* (12), 4675−4680.
(21) Misaghi, S.; Galardy, P. J.; Meester, W. J.; Ovaa, H.; Ploegh, H. L.; Gaudet, R. Structure of the ubiquitin hydrolase UCH-L3 complexed with a suicide substrate. *J. Biol. Chem.* **2005**, *280* (2), 1512−1520.
(22) Nishio, K.; Kim, S. W.; Kawai, K.; Mizushima, T.; Yamane, T.; Hamazaki, J.; Murata, S.; Tanaka, K.; Morimoto, Y. Crystal structure of the de-ubiquitinating enzyme UCH37 (human UCH-L5) catalytic domain. *Biochem. Biophys. Res. Commun.* **2009**, *390* (3), 855−860.
(23) Artavanis-Tsakonas, K.; Weihofen, W. A.; Antos, J. M.; Coleman, B. I.; Comeaux, C. A.; Duraisingh, M. T.; Gaudet, R.; Ploegh, H. L. Characterization and structural studies of the Plasmodium falciparum ubiquitin and Nedd8 hydrolase UCHL3. *J. Biol. Chem.* **2010**, *285* (9), 6857−6866.
(24) Navarro, M. F.; Carmody, L.; Romo-Fewell, O.; Lokensgard, M. E.; Love, J. J. Characterizing substrate selectivity of ubiquitin C-terminal hydrolase-L3 using engineered alpha-linked ubiquitin substrates. *Biochemistry* **2014**, *53* (51), 8031−8042.
(25) Johnston, S. C.; Larsen, C. N.; Cook, W. J.; Wilkinson, K. D.; Hill, C. P. Crystal structure of a deubiquitinating enzyme (human UCH-L3) at 1.8 Å resolution. *EMBO J.* **1997**, *16* (13), 3787−3796.
(26) Rajesh, S.; Sakamoto, T.; Iwamoto-Sugai, M.; Shibata, T.; Kohno, T.; Ito, Y. Ubiquitin binding interface mapping on yeast ubiquitin hydrolase by NMR chemical shift perturbation. *Biochemistry* **1999**, *38* (29), 9242−9253.
(27) Cordier, F.; Grzesiek, S. Direct Observation of Hydrogen Bonds in Proteins by Interresidue $^{3h}J_{NC'}$ Scalar Couplings. *J. Am. Chem. Soc.* **1999**, *121* (7), 1601−1602.
(28) Gottstein, D.; Kirchner, D. K.; Güntert, P. Simultaneous single-structure and bundle representation of protein NMR structures in torsion angle space. *J. Biomol. NMR* **2012**, *52* (4), 351−364.
(29) Popp, M. W.; Artavanis-Tsakonas, K.; Ploegh, H. L. Substrate filtering by the active site crossover loop in UCHL3 revealed by sortagging and gain-of-function mutations. *J. Biol. Chem.* **2009**, *284* (6), 3593−3602.
(30) Häussinger, D.; Huang, J. R.; Grzesiek, S. DOTA-M8: An extremely rigid, high-affinity lanthanide chelating tag for PCS NMR spectroscopy. *J. Am. Chem. Soc.* **2009**, *131* (41), 14761−14767.
(31) Yang, Y.; Yang, F.; Gong, Y. J.; Chen, J. L.; Goldfarb, D.; Su, X. C. A Reactive, Rigid Gd(III) Labeling Tag for In-Cell EPR Distance Measurements in Proteins. *Angew. Chem., Int. Ed. Engl.* **2017**, *56* (11), 2914−2918.
(32) Yang, Y.; Wang, J. T.; Pei, Y. Y.; Su, X. C. Site-specific tagging proteins via a rigid, stable and short thiolether tether for paramagnetic spectroscopic analysis. *Chem. Commun.* **2015**, *51* (14), 2824−2827.
(33) Theillet, F. X.; Binolfi, A.; Bekei, B.; Martorana, A.; Rose, H. M.; Stuiver, M.; Verzini, S.; Lorenz, D.; van Rossum, M.; Goldfarb, D.; et al. Structural disorder of monomeric alpha-synuclein persists in mammalian cells. *Nature* **2016**, *530* (7588), 45−50.
(34) Berliner, L. J.; Grunwald, J.; Hankovszky, H. O.; Hideg, K. A novel reversible thiol-specific spin label: Papain active site labeling and inhibition. *Anal. Biochem.* **1982**, *119* (2), 450−455.
(35) Ottiger, M.; Delaglio, F.; Bax, A. Measurement of J and dipolar couplings from simplified two-dimensional NMR spectra. *J. Magn. Reson.* **1998**, *131* (2), 373−378.
(36) Kitao, A.; Wagner, G. A space-time structure determination of human CD2 reveals the CD58-binding mode. *Proc. Natl. Acad. Sci. U. S. A.* **2000**, *97* (5), 2064−2068.
(37) Kitao, A.; Wagner, G. Amplitudes and directions of internal protein motions from a JAM analysis of ^{15}N relaxation data. *Magn. Reson. Chem.* **2006**, *44* (S1), S130−S142.
(38) Igarashi, S.; Osawa, M.; Takeuchi, K.; Ozawa, S.; Shimada, I. Amino acid selective cross-saturation method for identification of proximal residue pairs in a protein-protein complex. *J. Am. Chem. Soc.* **2008**, *130* (36), 12168−12176.
(39) Tollinger, M.; Skrynnikov, N. R.; Mulder, F. A.; Forman-Kay, J. D.; Kay, L. E. Slow dynamics in folded and unfolded states of an SH3 domain. *J. Am. Chem. Soc.* **2001**, *123* (46), 11341−11352.
(40) Sakakibara, D.; Sasaki, A.; Ikeya, T.; Hamatsu, J.; Hanashima, T.; Mishima, M.; Yoshimasu, M.; Hayashi, N.; Mikawa, T.; Walchli, M.; et al. Protein structure determination in living cells by in-cell NMR spectroscopy. *Nature* **2009**, *458* (7234), 102−105.
(41) Tanaka, T.; Ikeya, T.; Kamoshida, H.; Suemoto, Y.; Mishima, M.; Shirakawa, M.; Güntert, P.; Ito, Y. High-Resolution Protein 3D Structure Determination in Living Eukaryotic Cells. *Angew. Chem., Int. Ed. Engl.* **2019**, *58* (22), 7284−7288.

https://doi.org/10.1021/jacs.5c06502
J. Am. Chem. Soc. 2025, 147, 29884−29894